Tailored quinones support high-turnover Pd catalysts for oxidative C–H arylation with O_2

Authors: Chase A. Salazar,[1] Kaylin N. Flesch,[1] Brandon E. Haines,[2] Philip S. Zhou,[1] Djamaladdin G. Musaev,[2] and Shannon S. Stahl[1]*

Affiliations:

[1] Department of Chemistry, University of Wisconsin-Madison, 1101 University Avenue, Madison, Wisconsin 53706, United States.

[2] Cherry L. Emerson Center for Scientific Computation, Emory University, 1515 Dickey Drive, Atlanta, Georgia 30322, United States

*Correspondence to: stahl@chem.wisc.edu

Abstract:

Palladium(II)-catalyzed C–H oxidation reactions could streamline the synthesis of pharmaceuticals, agrochemicals, and other complex organic molecules. Existing methods, however, commonly exhibit poor catalyst performance with high Pd loading (e.g., 10 mol%) and a need for (super)stoichiometric quantities of undesirable oxidants, such as benzoquinone and silver(I) salts. The present study probes the mechanism of a representative Pd-catalyzed oxidative C–H arylation reaction and elucidates mechanistic features that undermine catalyst performance, including substrate-consuming side reactions and sequestration of the catalyst as inactive species. Systematic tuning of the quinone co-catalyst overcomes these deleterious features. Use of 2,5-di-*tert*-butyl-*p*-benzoquinone enables efficient use of molecular oxygen as the oxidant, high reaction yields, and >1900 turnovers by the palladium catalyst.

One Sentence Summary: Mechanistic studies lead to a high-performance palladium/quinone co-catalyst system for oxidative C–H arylation using O_2 as the oxidant.

Main Text:

Homogeneous palladium-catalyzed oxidation reactions of organic molecules originated in 1959 with the discovery of the Wacker process for oxidative coupling of ethylene and water (*1*). Pd-catalyzed C–H oxidation reactions for oxidative homocoupling of arenes to biaryls were reported shortly thereafter (*2*), including examples compatible with O_2 as the terminal oxidant (*3*). The poor catalytic efficiency and low regioselectivity of these methods contributed to development of Pd-catalyzed cross-coupling reactions with pre-oxidized substrates, such as aryl halides, as coupling partners. While Pd-catalyzed cross-coupling reactions have achieved extraordinary success (*4*), methods for direct oxidative functionalization of C–H bonds could substantially streamline synthetic access to diverse chemical structures (*5*-*8*).

Most $Pd^{II/0}$-catalyzed coupling reactions, including both oxidative and non-oxidative examples, fit into two general classes: (i) olefinations, such as Heck, Fujiwara-Moritani, and related reactions that involve coupling with alkenes and generate products via β-hydride elimination from a Pd^{II}-alkyl intermediate, and (ii) arylations, such as Suzuki-Miyaura, Negishi, and related reactions that involve coupling with arenes or aryl nucleophiles and generate the products via reductive elimination from a Pd^{II}–aryl intermediate. The oxidative reactions (cf. Fig. 1A) are mechanistically similar to non-oxidative cross-coupling reactions, but they often exhibit worse catalytic performance and require the use of one or more stoichiometric oxidants, such as Cu^{II}, Ag^{I}, and benzoquinone. The representative collection of oxidative arylation reactions in Fig. 1B, emphasizing cases in which the C–H substrate is the limiting reagent, highlights typical catalytic turnover numbers and stoichiometric oxidant(s) (*9*-*16*). The initial indole arylation example (*9*) achieves comparatively high turnovers (32 TOs); however, it requires 3 equiv $Cu(OAc)_2$ as the oxidant and 30 equiv

of benzene as a coupling partner. Many other examples feature < 10 TOs (see Fig. S1A in the Supplementary Materials for additional examples). Oxidative olefination reactions with limiting C–H substrate often exhibit similarly poor catalytic performance (see Fig. S1B in the Supplementary Materials for examples). We have noted, however, that Pd-catalyzed oxidation reactions that proceed via β-hydride elimination tend to be more compatible with O_2 as an oxidant than reductive elimination reactions (*17*). This phenomenon is clearly demonstrated in a pair of reactions reported by Yu and coworkers involving $Pd^{II/0}$-catalyzed C–H olefination (*18-20*) and arylation (*21*). Both were demonstrated with 1 atm O_2 as the oxidant, but the olefination reaction accessed 455 TOs (Fig. 1C, left), whereas the arylation reaction (Fig. 1C, right) achieved only 13 TOs under comparable conditions. Understanding the factors that limit catalyst turnovers in oxidative arylation reactions of this type could play a major role in expanding their

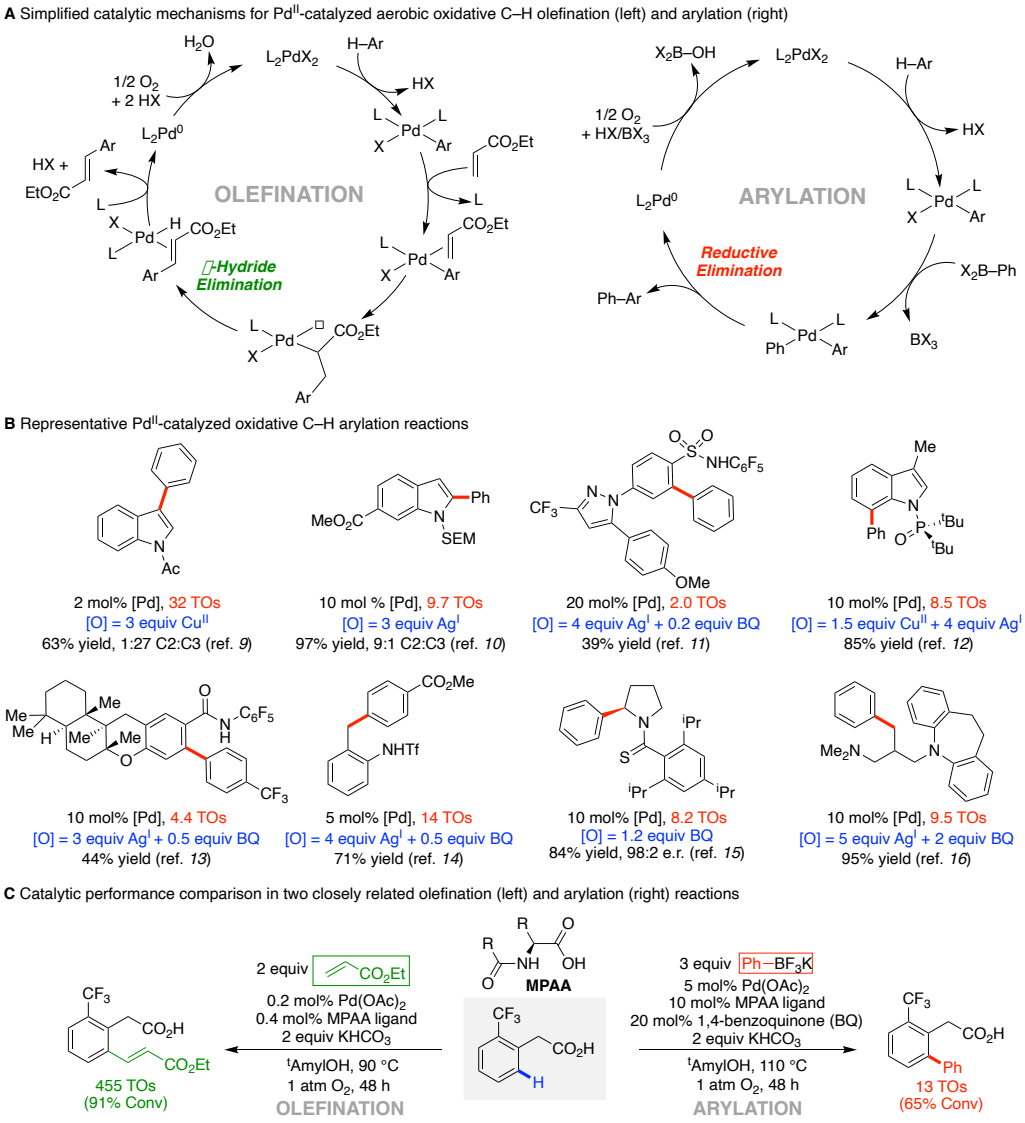

Fig. 1. Pd-catalyzed aerobic C–H oxidation reactions, highlighting challenges in catalyst performance. (**A**) Mechanisms for Pd^{II}-catalyzed oxidative olefination and arylation reactions using O_2 as the oxidant. (**B**) Catalytic metrics for representative oxidative arylation reactions (*9-16*). (**C**) Comparison of catalyst turnovers in Pd-catalyzed olefination and arylation reactions (*19*, *21*). MPAA = Mono-*N*-protected amino acid.

utility, and accessing improved catalytic performance could set the stage for large-scale applications that would greatly benefit from low catalyst loading and use of O_2 as an oxidant (*22*). Here, we present a mechanistic study of the Pd-catalyzed C–H arylation reaction in Fig. 1C and use the insights to develop a modified catalyst system capable of accessing >1900 TOs and high yields with O_2 as the oxidant.

The reported arylation reaction in Fig. 1C was adapted to facilitate mechanistic study. Use of the potassium salt of the arene substrate [2-(trifluoromethyl)phenylacetic acid (**1**)] eliminated the requirement for heterogeneous $KHCO_3$ as a Brønsted base, and arylboronic acid pinacol ester (**2**) provided a soluble alternative to the $ArBF_3K$ coupling partner. An 83% NMR assay yield of the arylation product **3** was obtained with these modifications when the reaction was conducted with 1 atm O_2 (Fig. 2A), representing an improvement over the originally reported yield of 65%. The initial experiments confirmed that 1,4-benzoquinone (BQ) is a crucial co-catalyst for the reaction. In the absence of BQ, negligible arylation product was formed, with the majority of the arylboronate undergoing protodeboronation to afford fluorobenzene (Ar^F–H) (Fig. 2A). Analysis of the reaction time course revealed a kinetic burst at the start of the reaction, with a magnitude corresponding to one turnover of the Pd catalyst, followed by a much slower steady-state rate (Fig. 2B). Increasing the oxygen pressure had no effect on the burst, but it led to an increase in rate following the burst roughly proportional to the change in O_2 pressure (0.46×10^{-3} mM/s at 1 atm; 2.5×10^{-3} at 6.4 atm).

The two-stage catalytic mechanism in Fig. 2C provided a framework for preliminary interpretation of these results. The kinetic burst could arise from fast stoichiometric oxidative coupling of the substrates by Pd^{II}/BQ, while the post-burst phase could arise from turnover-limiting aerobic oxidation of the reduced Pd catalyst. BQ is commonly used to oxidize Pd^0 in Pd-catalyzed oxidation reactions (*23*); however, Brønsted acid is needed to promote this reaction (*24*). We speculated that the basic conditions associated with the present arylation reaction prevent BQ from serving as an effective oxidant, and it instead coordinates to Pd^0 and inhibits its reoxidation by O_2. This mechanistic hypothesis prompted us to test sterically modified benzoquinone derivatives that might undergo more facile displacement by O_2 (Fig. 2D) (*25*), thereby facilitating catalytic turnover. Use of *tert*-butyl-*p*-benzoquinone (^{t}BuBQ) had virtually no impact on the reaction time course; the reaction still exhibited a kinetic burst, followed by slow steady-state turnover. In contrast, use of 2,5-di-*tert*-butyl-*p*-benzoquinone (2,5-^{t}Bu$_2$BQ) led to a sustained high rate, without a slowdown after the initial catalyst turnover (Fig. 2D, blue).

The reaction was then interrogated by ^{19}F NMR spectroscopy in order to gain insights into the role of the different catalyst components. The C–H substrate **1** and $Pd^{II}(OAc)_2$ were dissolved in ^{t}AmylOH and added to an NMR tube under ambient air. No reaction was observed upon warming this mixture to 64 °C, consistent with previous results showing that C–H activation is very slow in the absence of a mono-*N*-protected amino acid (MPAA) ligand (*8,19,26,27*). Addition of the MPAA ligand initiated immediate formation of the previously characterized palladacycle derived from activation of the substrate C–H bond (Fig. 2E, black, see Supplementary Materials Section 5 for details) (*27*). Subsequent addition of the arylboronic ester coupling partner led to formation of protodeboronation side product, Ar^F–H (Fig. 2E, blue). No C–H arylation product **3** was observed at this stage, but arose only after addition of 2,5-^{t}Bu$_2$BQ (Fig. 2E, red). These observations align with the catalytic data in Fig. 2A showing that Ar^F–H is the product obtained when the reaction is conducted in the absence of BQ. Systematic variation of the 2,5-^{t}Bu$_2$BQ concentration provided evidence for direct competition between the formation of Ar^F–H and **3**, with the latter promoted by higher quinone concentrations (Fig. 2F).

These experiments were further complemented by spectroscopic and kinetic analysis of the fully constituted catalytic reaction mixture. Use of a sealed NMR tube with higher initial O_2 pressure (6.9 atm) minimized complications arising from depletion of dissolved O_2 in the NMR solution (e.g., which accounts for decay of the palladacycle after 2.5 h in Fig. 2E). Under these conditions, the palladacycle forms rapidly and accounts for all of the Pd in solution (Fig. 2G, see Supplementary Materials Section 6 for details). This

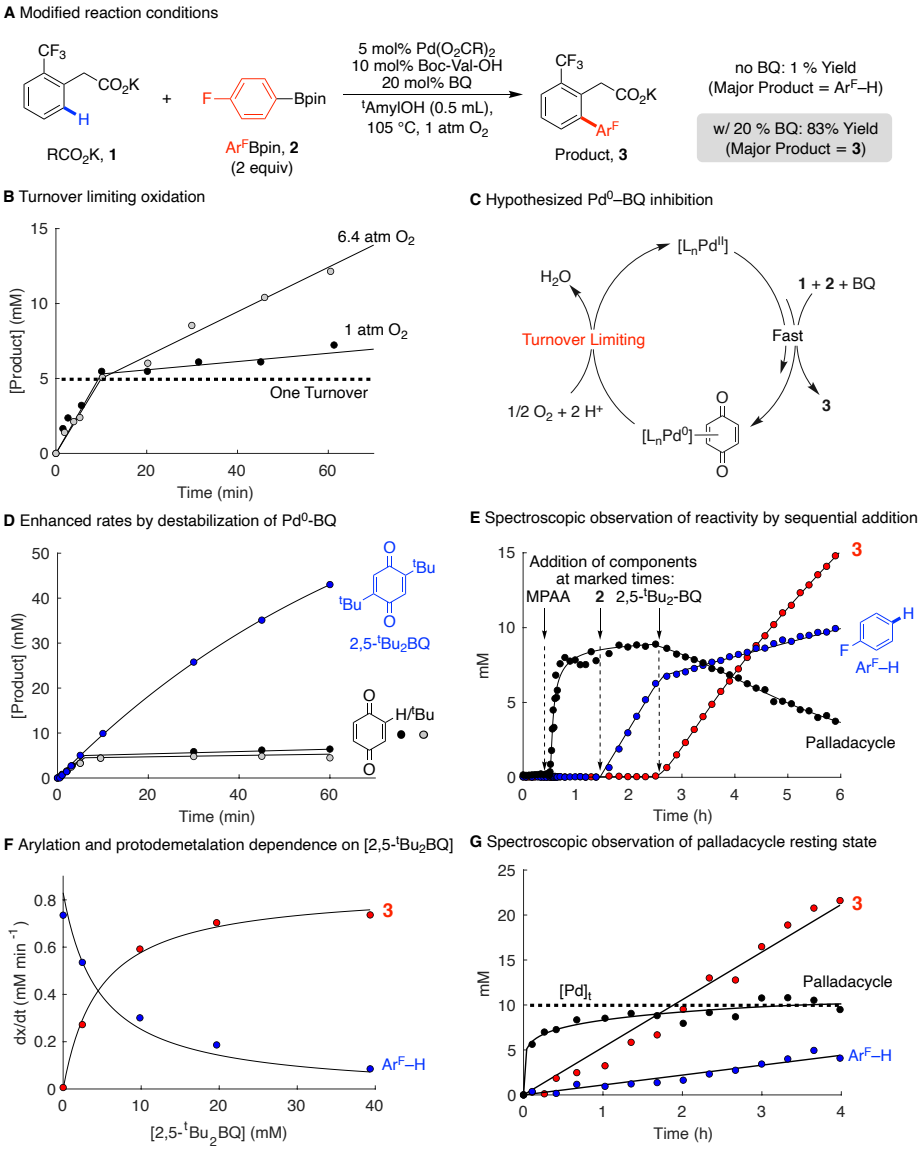

Fig. 2. Kinetic and spectroscopic analysis of the Pd-catalyzed C–H arylation reaction. (**A**) Oxidative arylation conditions (R = 2-(trifluoromethyl)$C_6H_4CH_2$-). (**B**) Kinetic data showing a burst and the influence of O_2 pressure on the steady state arylation rate. (**C**) Simplified mechanism rationalizing the kinetic burst and BQ inhibition of steady state turnover. (**D**) Enhanced steady state rate observed with 2,5-^{t}Bu$_2$BQ. (**E**) Reaction progress obtained from ^{19}F NMR spectroscopic analysis of the reaction mixture to which different reaction components were added sequentially. Interpolative curve fits are included as a guide. (**F**) Kinetic data [2,5-^{t}Bu$_2$BQ] for formation of **3** and Ar^F–H, with correlations reflecting a hyperbolic curve fit [y = ax/(1 + bx)]. (**G**) Spectroscopic observation of palladacycle resting state under 6.9 atm O_2, with linear and interpolative curve fits as a guide. Conditions: (**A**) [**1**] = 200 mM, 24 h (**B**, **D**, **F**) [**1**] = 100 mM, $[Pd]_t$ = 5 mM, [Boc-Val-OH] = 10 mM, [quinone] = 20 mM, 85 °C, 1 mL, 1 atm O_2. (**E**, **G**) [**1**] = 100 mM, $[Pd]_t$ = 10 mM, [Boc-Val-OH] = 20 mM, [2,5-^{t}Bu$_2$BQ] = 40 mM, 64 °C, 0.55 mL.

species persists as the catalyst resting state, while the arylation product **3** steadily appears in parallel with smaller quantities of the Ar^F–H byproduct. Initial-rate kinetic studies revealed a negligible deuterium kinetic isotope effect (k_H/k_D = 1.2 ± 0.1), based on independent rates measured for arylation of **1** and **1**-d_1, the latter deuterated at the site targeted by C–H activation, ortho to the directing group. Under conditions

of saturating [2,5-^{t}Bu$_2$BQ], the catalytic rate law exhibits a first-order dependence on [Pd], a zero-order dependence on O_2 pressure, and saturation dependences on the coupling partners [**1**] and [**2**] (Figs. S2, S8-10 in the Supplementary Materials).

The experimental data presented above indicate that the palladacycle is the catalyst resting state and transmetalation of Ar^F from the arylboronate to palladium is the turnover-limiting step when 2,5-^{t}Bu$_2$BQ is used as the quinone co-catalyst. The dependence of the rate on substrate **1** is rationalized by the ability of basic additives to promote the transmetalation step (*28*). The proposed mechanism in Fig. 3A incorporates these features, together with other steps in the catalytic reaction and steps leading to byproduct formation. The reaction is initiated by MPAA-promoted C–H activation of the substrate in **I** to form palladacycle **II** (*26*), which is observed by ^{19}F NMR spectroscopy. A recent study indicates that the MPAA ligand plays a catalytic role in the C–H activation step and does not influence other steps in the mechanism (*27*). Moreover, MPAA undergoes facile exchange with substrate-derived carboxylates and likely does not remain coordinated to Pd throughout the cycle. Transmetalation from the arylboronate to the palladacycle generates the diaryl-Pd^{II} species **III**, which can undergo protodemetalation to form byproduct Ar^F–H and regenerate the palladacycle **II** or undergo quinone-promoted reductive elimination to generate the arylation product **3** and the Pd^0-quinone adduct **IV**. The Pd^{II} catalyst is regenerated via reaction of **IV** with O_2.

The proposed mechanism in Fig. 3A highlights the delicate balance between the beneficial and deleterious effects of the quinone co-catalyst. It is needed to promote reductive elimination (*29-31*) and avoid catalytic degradation of the arylboronate; however, it can also inhibit catalytic turnover by coordinating too strongly to Pd^0. Further insights into these roles of quinone were obtained from density functional theory calculations (Fig. 3b). The relative energies presented in Fig. 3B were calculated at the M06-(IEF-PCM)/BS2 [BS2 = 6-311+G(d,p) (for all atoms except Pd) and SDD (for Pd)] levels of theory by using geometries and enthalpy and entropy corrections calculated at the B3LYP-D3BJ/BS1 level of theory [BS1 = 6-31G(d,p) (for all atoms except Pd) and LanL2dz (for Pd)] (see Section 8 in the Supplementary Materials for details).

Specifically, the Pd^{II}-diaryl species, Pd(Ar)(Ar') (cf. **III** in Fig. 3A) was interrogated to compare the energetics of the protodemetalation step with C–C reductive elimination in the absence and presence of quinone (BQ and 2,5-^{t}Bu$_2$BQ) (Fig. 3b). Neither BQ nor 2,5-^{t}Bu$_2$BQ form favorable adducts with the Pd(Ar)(Ar') species ($\Delta G°$ = +2.9 and =3.9 kcal/mol, respectively); however, both lower the kinetic barrier for reductive elimination relative to the quinone-free barrier ($\Delta\Delta G^‡$ = –4.4 and –3.2 kcal/mol for BQ and 2,5-^{t}Bu$_2$BQ). The transition-state energies for quinone-promoted reductive elimination is very similar to the transition-state energy for the protodemetalation pathway, consistent with the competitive formation of Ar^F–H and product **3** (cf. Fig. 2f).

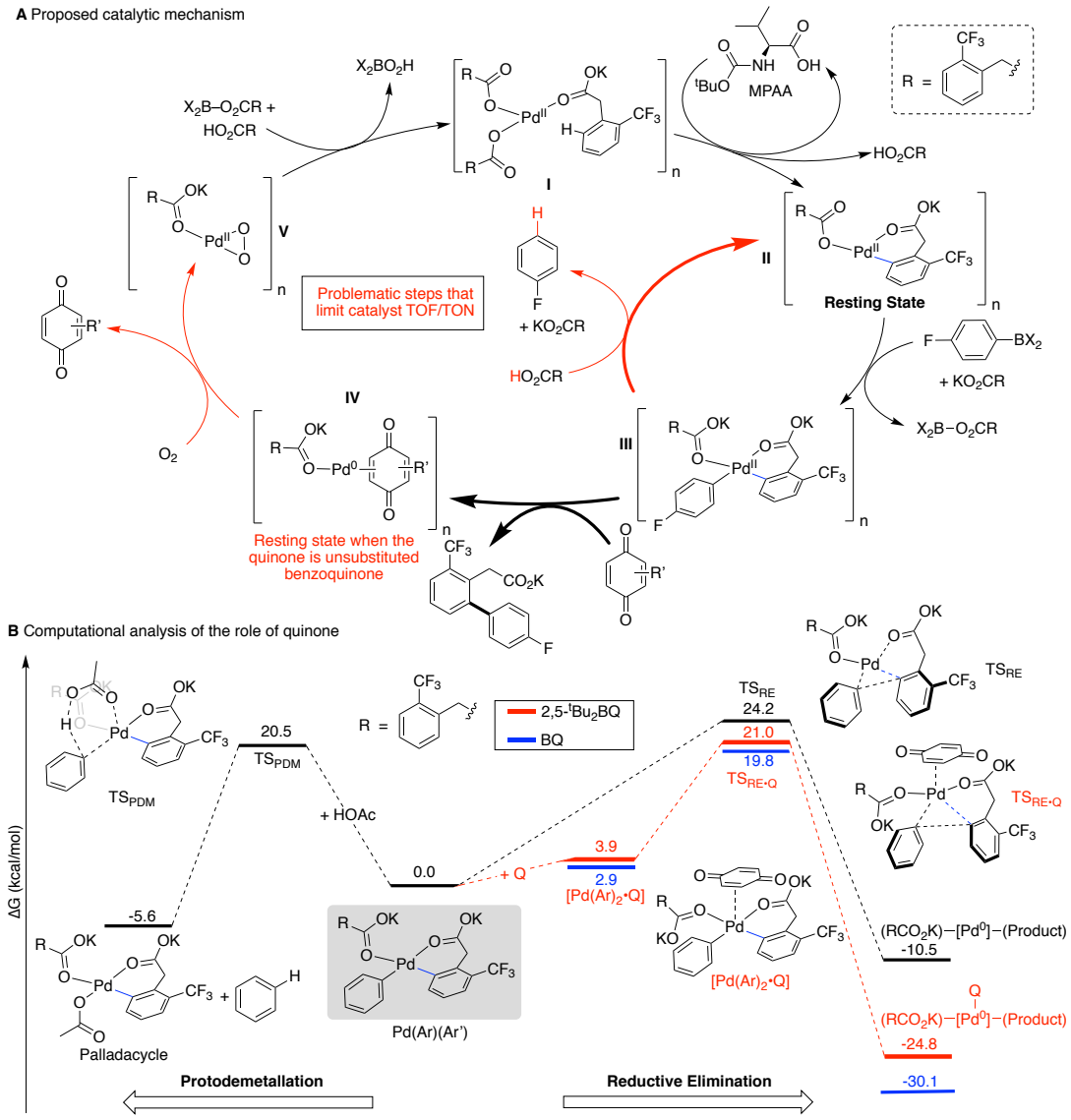

Fig. 3. Catalytic cycle consistent with the experimental data and computational analysis. (**A**) The proposed catalytic mechanism for C–H arylation of **1** (R = 2-(trifluoromethyl)$C_6H_4CH_2$-), and (**B**) calculated free energy diagram for protodemetalation and reductive elimination pathways in the absence and presence of quinones. See text and Supplementary Materials for details of the computational methods. TOF = Turnover Frequency, TON = Turnover Numbers

The mechanistic insights provided above set the stage for efforts to optimize the catalytic performance. Key screening data are summarized in Fig. 4A, with full details provided in Section 9 of the Supplementary Materials. Use of 2,5-^{t}Bu$_2$BQ with 5% mol Pd(OAc)$_2$ and 3 atm O_2 led to >99% yield of **3**, corresponding 20 TOs (Fig. 4a, entry 1). Reducing the catalyst loading to 0.15 mol% Pd with the same ratio of Pd:MPAA:2,5-^{t}Bu$_2$BQ (1:2:4) resulted in 147 TOs. The reaction instead generated large quantities of Ar^F–H and 4,4'-difluorobiphenyl (Ar^F–Ar^F) (entry 2). The latter byproduct arises from oxidative homocoupling of arylboronate (*32*) and is rationalized by inefficient C–H activation of **1** at low Pd/MPAA loading, due to relatively weak binding of MPAA to Pd^{II} (27). This complication was addressed by increasing the MPAA loading to 10 mol%, which enhances the rate of C–H activation without increasing the Pd loading. These conditions supported effective C–H activation and increased the Pd TOs to 373 (Fig. 4a, entry 3). The quinone loading and identity of the MPAA ligand were then varied in order to access higher reaction yields. The most dramatic effect was observed upon replacing Boc-Val-OH with Ac-Ile-OH as the MPAA ligand, which led to 667 TOs and a quantitative yield of **3** (entry 5).

With the identification of conditions compatible with low Pd loading, we revisited the influence of the quinone identity. The results reinforced previous observations (Fig. 4b). Little product was observed with the parent BQ and with ^{t}BuBQ (**A** and **B**), while higher catalytic turnover was evident with 2,5-Me$_2$BQ (**C**, 230 TOs). Further increase in the number or size of the substituents conferred additional benefits, as evident with Me$_4$BQ (**F**, 574 TOs) and 2,6-^{t}Bu$_2$BQ, and 2,5-^{t}Bu$_2$BQ (**G** and **H**, 667 TOs). The latter two examples led to quantitative product yield at 0.15 mol% Pd loading, prompting reassessment with 0.05 mol% Pd. The beneficial effect of these sterically encumbered quinones is evident from the 1520 turnovers with the 2,6-^{t}Bu$_2$BQ and 1960 turnovers with the 2,5-^{t}Bu$_2$BQ, the latter corresponding to a near-quantitative product yield.

This survey also provided an opportunity to test an unexpected conclusion of the mechanistic studies above. The proposed catalytic mechanism in Fig. 3A features a non-redox role for the quinone, suggesting that redox-inactive electron-deficient alkenes should also support catalytic turnover. This hypothesis was validated by the use of dimethyl fumarate (**D**) and diisopropyl fumarate (**E**), which supported 390 and 440 turnovers respectively. Although this performance is not better than that observed with the sterically encumbered quinones (**F–H**), it is much better than BQ, the most commonly used co-catalyst in Pd-catalyzed aerobic oxidation reactions.

The optimized catalyst conditions were tested with a representative collection of other substrate partners with 0.5 mol% Pd (Fig. 4C). Several arylboronic esters, including methyl benzoate and protected aniline derivatives, and methylboronic acid react with the parent C–H substrate in good-to-excellent isolated yields (**4–7**). The 1-naphthylacetate and benzoate C–H substrates (**8–10**) also proceed in good yield. Substrates with neutral nitrogen direction groups, including the rather heterocyclic sildenafil precursor, were also effective (**11**, **12**), albeit with more modest yields.

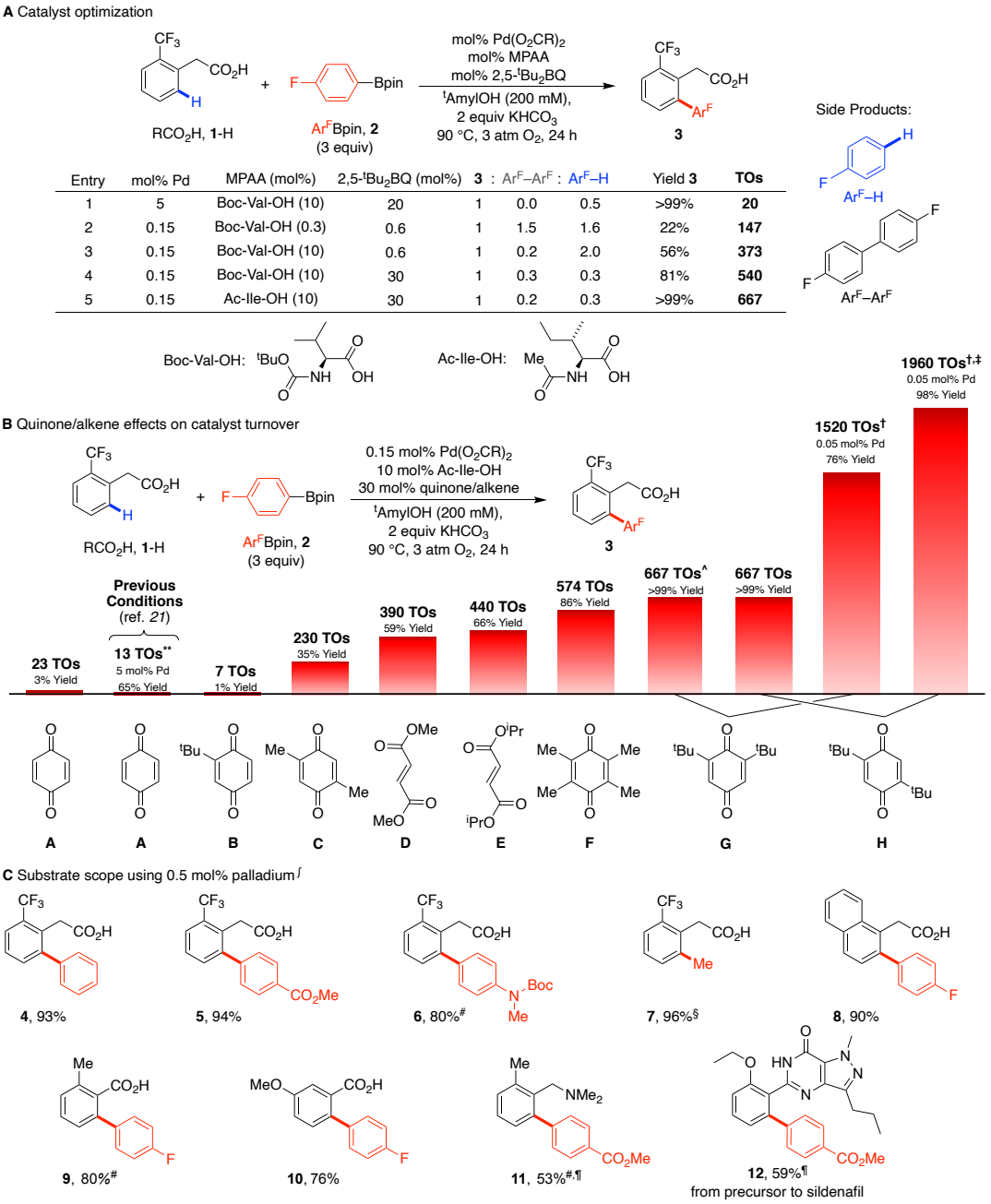

Entry	mol% Pd	MPAA (mol%)	2,5-^{t}Bu$_2$BQ (mol%)	3	Ar^F–Ar^F	Ar^F–H	Yield 3	TOs
1	5	Boc-Val-OH (10)	20	1	0.0	0.5	>99%	**20**
2	0.15	Boc-Val-OH (0.3)	0.6	1	1.5	1.6	22%	**147**
3	0.15	Boc-Val-OH (10)	0.6	1	0.2	2.0	56%	**373**
4	0.15	Boc-Val-OH (10)	30	1	0.3	0.3	81%	**540**
5	0.15	Ac-Ile-OH (10)	30	1	0.2	0.3	>99%	**667**

Fig. 4. Catalytic performance with low catalyst loading. (**A**) Catalyst optimization data showing product ratios and catalyst turnover numbers (TON) for the oxidative coupling of **1** and **2**. (**B**) Observed turnovers of **3** with different quinones/alkenes. (**C**) Application of mechanistic insights to other substrates and coupling partners. Conditions: (**A**,**B**) see conditions shown in above and below the arrow in A and **B**, 0.5 mL scale, Data based on NMR assay yield. (**C**) Identical to the conditions used in B except 0.5 mol% Pd was used with 30 mol% 2,5-^{t}Bu$_2$BQ. [**] Reported catalyst turnovers with 5 mol % $Pd(OAc)_2$ and 20 mol % BQ (*21*). [^] A 93% isolated yield was obtained. [†] with 0.05 mol% $Pd(O_2CR)_2$ and 72 hours reaction time. [‡] A 96% isolated yield was obtained. [∫] Yields shown are isolated product yields. [#] 30 mol% 2,6-^{t}Bu$_2$BQ was used. [§] 5 equivalents of methylboronic acid was used. [¶] K_2CO_3 was used as the base and no Ac-Ile-OH added.

Overall, the results above highlight the delicate balancing act of quinone co-catalysts in these reactions. The quinone is needed to promote the kinetically difficult reductive elimination step and prevent deleterious consumption of the arylboronate via protodemetalation, but it also must avoid catalytic inhibition, which can arise if it coordinates too strongly to Pd^0. Tuning of the quinone structure allows an effective balance to be found among these roles. These considerations provide relevant context for comparison with the closely related olefination reactions (Fig. 1A and 1C). The β-hydride elimination and H–X reductive elimination steps in olefination reactions are kinetically more facile than the C–C reductive elimination step in the arylation reactions, and olefination reactions lack the deleterious protodemetalation side-reaction that hinders the arylation reaction. Thus, olefinations often do not employ a quinone co-catalyst and tend to be more amenable to aerobic catalytic turnover. The insights from this study show how strategic integration of a redox inactive quinone or related co-catalyst in Pd-catalyzed arylation reactions could provide the basis for highly effective catalytic performance, enabling low Pd loading and effective use of O_2 as the oxidant. The promising extension of these results to other substrates (Fig. 4C) set the stage for further application of the concepts described herein.

References

(*1*) J. Smidt, W. Hafner, R. Jira, J. Sedlmeier, R. Sieber, R. Rüttinger, H. Kojer, Katalytische umsetzungen von olefinen an platinmetall-verbindungen das consortium-verfahren zur herstellung von acetaldehyd. *Angew. Chem*. **71**, 176–182 (1959).

(*2*) R. van Helden, G. Verberg, The oxidative coupling of aromatic compounds with palladium salts. *Rec. Trav. Chim. Pays-Bas*. **84**, 1263–1273 (1965).

(*3*) S. S. Stahl, Palladium oxidase catalysis: Selective oxidation of organic chemicals by direct dioxygen-coupled turnover. *Angew. Chem. Int. Ed.* **43**, 3400–3420 (2004).

(*4*) C. C. C. Johansson-Seechurn, M. O. Kitching, T. J. Colacot, V. Snieckus, Palladium-catalyzed cross-coupling: A historical contextual perspective to the 2010 Nobel Prize. *Angew. Chem. Int. Ed.* **51**, 5062–5085 (2012).

(*5*) X. Chen, K. M. Engle, D.-H. Wang, J.-Q. Yu, Palladium(II)-catalyzed C-H activation/C-C cross-coupling reactions: versatility and practicality. *Angew. Chem. Int. Ed*. **48**, 5094–5115 (2009).

(*6*) T. W. Lyons, M. S. Sanford, Palladium-catalyzed ligand-directed C−H functionalization reactions. *Chem. Rev.* **110**, 1147–1169 (2010).

(*7*) D. Wang, A. B. Weinstein, P. B. White, S. S. Stahl, Ligand-promoted palladium-catalyzed aerobic oxidation reactions. *Chem. Rev.* **118**, 2636–2679 (2017).

(*8*) J. He, M. Wasa, K. S. L. Chan, Q. Shao, J.-Q. Yu, Palladium-catalyzed transformations of alkyl C–H bonds. *Chem. Rev.* **117**, 8754–8786 (2017).

(*9*) D. R. Stuart, K. Fagnou, The catalytic cross-coupling of unactivated arenes. *Science*. **316**, 1172–1175 (2007).

(*10*) S. Potavathri, K. C. Pereira, S. I. Gorelsky, A. Pike, A. P. LeBris, B. DeBoef, Regioselective oxidative arylation of indoles bearing N-alkyl protecting froups: Dual C−H functionalization via a concerted metalation−deprotonation mechanism. *J. Am. Chem. Soc*. **132**, 14676–14681 (2010).

(*11*) H.-X. Dai, A. F. Stepan, M. S. Plummer, Y.-H. Zhang, J.-Q. Yu, Divergent C–H functionalizations directed by sulfonamide pharmacophores: Late-stage diversification as a tool for drug discovery. *J. Am. Chem. Soc.* **133**, 7222–7228 (2011).

(*12*) Y. Yang, X. Qiu, Y. Zhao, Y. Mu, Z. Shi, Palladium-catalyzed C–H arylation of indoles at the C7 position. *J. Am. Chem. Soc.* **138**, 495–498 (2016).

(*13*) B. R. Rosen, L. R. Simke, P. S. Thuy-Boun, D. D. Dixon, J.-Q. Yu, P. S. Baran, C–H functionalization logic enables synthesis of (+)-Hongoquercin A and related compounds. *Angew. Chem. Int. Ed.* **52**, 7317–7320 (2013).

(*14*) K. S. L. Chan, M. Wasa, L. Chu, B. N. Laforteza, M. Miura, J.-Q. Yu, Ligand-enabled cross-coupling of C(sp^3)–H bonds with arylboron reagents via Pd(II)/Pd(0) catalysis. *Nat. Chem*. **6**, 146–150 (2014).

(*15*) P. Jain, P. Verma, G. Xia, J.-Q. Yu, Enantioselective amine α-functionalization via palladium-catalysed C–H arylation of thioamides. *Nat. Chem*. **9**, 140–144 (2017).

(*16*) J. Rodrigalvarez, M. Nappi, H. Azuma, N. J. Flodén, M. E. Burns, M. J. Gaunt, Catalytic C(sp^3)–H bond activation in tertiary alkylamines. *Nat. Chem*. **12**, 76–81 (2020).

(*17*) A. N. Campbell, S. S. Stahl, Overcoming the "oxidant problem": Strategies to use O_2 as the oxidant in organometallic C–H oxidation reactions catalyzed by Pd (and Cu). *Acc. Chem. Res*. **45**, 851–863 (2012).

(*18*) D.-H. Wang, K. M. Engle, B.-F. Shi, J.-Q. Yu, Ligand-enabled reactivity and selectivity in a synthetically versatile aryl C–H olefination. *Science*. **327**, 315–319 (2010).

(*19*) K. M. Engle, D.-H. Wang, J.-Q. Yu, Ligand-accelerated C−H activation reactions: Evidence for a switch of mechanism. *J. Am. Chem. Soc.* **132**, 14137–14151 (2010).

(*20*) R. D. Baxter, D. Sale, K. M. Engle, J.-Q. Yu, D. G. Blackmond, Mechanistic rationalization of unusual kinetics in Pd-catalyzed C–H olefination. *J. Am. Chem. Soc.* **134**, 4600–4606 (2012).

(*21*) K. M. Engle, P. S. Thuy-Boun, M. Dang, J.-Q. Yu, Ligand-accelerated cross-coupling of C(sp^2)–H bonds with arylboron reagents. *J. Am. Chem. Soc.* **133**, 18183–18193 (2011).

(*22*) S. S. Stahl, P. L. Alsters, Liquid phase aerobic oxidation catalysis: Industrial applications and academic perspectives (Wiley-VCH Verlag GmbH & Co. KGaA, Weinheim, Germany, 2016)

(*23*) J.-E. Bäckvall, R. B. Hopkins, H. Grennberg, M. Mader, A. K. Awasthi, Multistep electron transfer in palladium-catalyzed aerobic oxidations via a metal macrocycle quinone system. *J. Am. Chem. Soc.* **112**, 5160–5166 (1990).

(*24*) H. Grennberg, A. Gogoll, J. E. Bäckvall, Acid-induced transformation of palladium(0)-benzoquinone complexes to palladium(II) and hydroquinone. *Organometallics*. **12**, 1790–1793 (1993).

(*25*) B. V. Popp, S. S. Stahl, "Oxidatively induced" reductive elimination of dioxygen from an η^2-peroxopalladium(II) complex promoted by electron-deficient alkenes. *J. Am. Chem. Soc.* **128**, 2804–2805 (2006).

(*26*) K. M. Engle, The mechanism of palladium(II)-mediated C–H cleavage with mono-N-protected amino acid (MPAA) ligands: Origins of rate acceleration. *Pure Appl. Chem.* **88**, 4520–20 (2016).

(*27*) C. A. Salazar, J. J. Gair, K. N. Flesch, I. A. Guzei, J. C. Lewis, S. S. Stahl, Catalytic behavior of mono-*N*-protected amino-acid ligands in ligand-accelerated C−H activation by palladium(II). *Angew. Chem. Int. Ed.* **59**, 10873–10877 (2020).

(*28*) A. J. J. Lennox, G. C. Lloyd-Jones, Selection of boron reagents for Suzuki–Miyaura coupling. *Chem. Soc. Rev.* **43**, 412–443 (2014).

(*29*) K. L. Hull, M. S. Sanford, Catalytic and highly regioselective cross-coupling of aromatic C−H substrates. *J. Am. Chem. Soc*. **129**, 11904–11905 (2007).

(*30*) I. A. Sanhueza, A. M. Wagner, M. S. Sanford, F. Schoenebeck, On the role of anionic ligands in the site-selectivity of oxidative C-H functionalization reactions of arenes. *Chem. Sci*. **4**, 2767–2775 (2013).

(*31*) A. Vasseur, J. Muzart, J. Le Bras, Ubiquitous Benzoquinones, Multitalented Compounds for Palladium-Catalyzed Oxidative Reactions. *Eur. J. Org. Chem*. **2015**, 4053–4069 (2015).

(*32*) C. Adamo, C. Amatore, I. Ciofini, A. Jutand, H. Lakmini, Mechanism of the Palladium-Catalyzed Homocoupling of Arylboronic Acids: Key Involvement of a Palladium Peroxo Complex. *J. Am. Chem. Soc*. **128**, 6829–6836 (2006).

(*33*) M. Takahashi, K. Masui, H. Sekiguchi, N. Kobayashi, A. Mori, M. Funahashi, N. Tamaoki, Palladium-catalyzed C−H homocoupling of bromothiophene derivatives and synthetic application to well-defined oligothiophenes. *J. Am. Chem. Soc.* **128**, 10930–10933 (2006).

(*34*) K. L. Hull, M. S. Sanford, Catalytic and highly regioselective cross-coupling of aromatic C−H substrates. *J. Am. Chem. Soc.* **129**, 11904–11905 (2007).

(*35*) D. R. Stuart, E. Villemure, K. Fagnou, Elements of regiocontrol in palladium-catalyzed oxidative arene cross-coupling. *J. Am. Chem. Soc*. **129**, 12072–12073 (2007).

(*36*) S. H. Cho, S. J. Hwang, S. Chang, Palladium-catalyzed C−H functionalization of pyridine *N*-oxides: Highly selective alkenylation and direct arylation with unactivated arenes. *J. Am. Chem. Soc.* **130**, 9254–9256 (2008).

(*37*) C.-Y. He, S. Fan, X. Zhang, Pd-catalyzed oxidative cross-coupling of perfluoroarenes with aromatic heterocycles. *J. Am. Chem. Soc.* **132**, 12850–12852 (2010).

(*38*) X. Zhao, C. S. Yeung, V. M. Dong, Palladium-catalyzed *ortho*-arylation of *o*-phenylcarbamates with simple arenes and sodium persulfate. *J. Am. Chem. Soc.* **132**, 5837–5844 (2010).

(*39*) S. Kirchberg, S. Tani, K. Ueda, J. Yamaguchi, A. Studer, K. Itami, Oxidative biaryl coupling of thiophenes and thiazoles with arylboronic acids through palladium catalysis: otherwise difficult C4-selective C-H arylation enabled by boronic acids. *Angew. Chem. Int. Ed.* **50**, 2387–2391 (2011).

(*40*) D. Mandal, A. D. Yamaguchi, J. Yamaguchi, K. Itami, Synthesis of Dragmacidin D via direct C–H couplings. *J. Am. Chem. Soc.* **133**, 19660–19663 (2011).

(*41*) D. G. Pintori, M. F. Greaney, Intramolecular oxidative C−H coupling for medium-ring synthesis. *J. Am. Chem. Soc.* **133**, 1209–1211 (2011).

(*42*) Z. Wang, K. Li, D. Zhao, J. Lan, J. You, Palladium-catalyzed oxidative C–H/C–H cross-coupling of indoles and pyrroles with heteroarenes. *Angew. Chem. Int. Ed*. **50**, 5365–5369 (2011).

(*43*) D.-W. Gao, Y.-C. Shi, Q. Gu, Z.-L. Zhao, S.-L. You, Enantioselective synthesis of planar chiral ferrocenes via palladium-catalyzed direct coupling with arylboronic acids. *J. Am. Chem. Soc.* **135**, 86–89 (2013).

(*44*) P. S. Thuy-Boun, G. Villa, D. Dang, P. Richardson, S. Su, J.-Q. Yu, Ligand-accelerated *ortho*-C–H alkylation of arylcarboxylic acids using alkyl boron reagents. *J. Am. Chem. Soc.* **135**, 17508–17513 (2013).

(*45*) K.-J. Xiao, D. W. Lin, M. Miura, R.-Y. Zhu, W. Gong, M. Wasa, J.-Q. Yu, Palladium(II)-catalyzed enantioselective C(sp^3)–H activation using a chiral hydroxamic acid ligand. *J. Am. Chem. Soc.* **136**, 8138–8142 (2014).

(*46*) C. He, M. J. Gaunt, Ligand-enabled catalytic C–H arylation of aliphatic amines by a four-membered-ring cyclopalladation pathway. *Angew. Chem. Int. Ed*. **54**, 15840–15844 (2015).

(*47*) Y. Cheng, G. Li, Y. Liu, Y. Shi, G. Gao, D. Wu, J. Lan, J. You, Unparalleled ease of access to a library of biheteroaryl fluorophores via oxidative cross-coupling reactions: Discovery of photostable NIR probe for mitochondria. *J. Am. Chem. Soc.* **138**, 4730–4738 (2016).

(*48*) D.-W. Gao, Q. Gu, S.-L. You, An enantioselective oxidative C–H/C–H cross-coupling reaction: Highly efficient method to prepare planar chiral ferrocenes. *J. Am. Chem. Soc.* **138**, 2544–2547 (2016).

(*49*) K.-J. Xiao, L. Chu, G. Chen, J.-Q. Yu, Kinetic resolution of benzylamines via palladium(II)-catalyzed C–H cross-coupling. *J. Am. Chem. Soc.* **138**, 7796–7800 (2016).

(*50*) C. Qi, W. Wang, K. D. Reichl, J. McNeely, J. A. Porco, Total synthesis of Aurofusarin: Studies on the atropisomeric stability of bis-naphthoquinones. *Angew. Chem. Int. Ed*. **57**, 2101–2104 (2018).

(*51*) Q. Shao, Q.-F. Wu, J. He, J.-Q. Yu, Enantioselective γ-C(sp^3)–H activation of alkyl amines via Pd(II)/Pd(0) catalysis. *J. Am. Chem. Soc.* **140**, 5322–5325 (2018).

(*52*) L. Hu, P.-X. Shen, Q. Shao, K. Hong, J. X. Qiao, J.-Q. Yu, Pd^{II}-catalyzed enantioselective C(sp^3)−H activation/cross-coupling reactions of free carboxylic acids. *Angew. Chem. Int. Ed*. **58**, 2134–2138 (2019).

(*53*) M. Ye, G.-L. Gao, J.-Q. Yu, Ligand-promoted C-3 selective C–H olefination of pyridines with Pd catalysts. *J. Am. Chem. Soc.* **133**, 6964–6967 (2011).

(*54*) G. Yang, P. Lindovska, D. Zhu, J. Kim, P. Wang, R.-Y. Tang, M. Movassaghi, J.-Q. Yu, Pd(II)-catalyzed *meta*-C–H olefination, arylation, and acetoxylation of indolines using a U-shaped template. *J. Am. Chem. Soc.* **136**, 10807–10813 (2014).

(*55*) J. He, S. Li, Y. Deng, H. Fu, B. N. Laforteza, J. E. Spangler, A. Homs, J.-Q. Yu, Ligand-controlled C(sp^3)–H arylation and olefination in synthesis of unnatural chiral α–amino acids. *Science*. **343**, 1216 (2014).

(*56*) A. Deb, S. Bag, R. Kancherla, D. Maiti, Palladium-catalyzed aryl C–H olefination with unactivated, aliphatic alkenes. *J. Am. Chem. Soc.* **136**, 13602–13605 (2014).

(*57*) J. Calleja, D. Pla, T. W. Gorman, V. Domingo, B. Haffemayer, M. J. Gaunt, A steric tethering approach enables palladium-catalysed C–H activation of primary amino alcohols. *Nat. Chem*. **7**, 1009–1016 (2015).

(*58*) H. Jiang, J. He, T. Liu, J.-Q. Yu, Ligand-enabled γ-C(sp^3)–H olefination of amines: en route to pyrrolidines. *J. Am. Chem. Soc.* **138**, 2055–2059 (2016).

(59) Q.-J. Liang, C. Yang, F.-F. Meng, B. Jiang, Y.-H. Xu, T.-P. Loh, Chelation versus non-chelation control in the stereoselective alkenyl sp^2 C−H bond functionalization reaction. *Angew. Chem. Int. Ed.* **56**, 5091–5095 (2017).

(*60*) B. J. Gorsline, L. Wang, P. Ren, B. P. Carrow, C–H alkenylation of heteroarenes: Mechanism, rate, and selectivity changes enabled by thioether ligands. *J. Am. Chem. Soc.* **139**, 9605–9614 (2017).

(*61*) Z. Zhang, K. Tanaka, J.-Q. Yu, Remote site-selective C–H activation directed by a catalytic bifunctional template. *Nature*. **543**, 538–542 (2017).

(*62*) P. Wang, P. Verma, G. Xia, J. Shi, J. X. Qiao, S. Tao, P. T. W. Cheng, M. A. Poss, M. E. Farmer, K.-S. Yeung, J.-Q. Yu, Ligand-accelerated non-directed C–H functionalization of arenes. *Nature*. **551**, 489–493 (2017).

(*63*) Z. Zhuang, C.-B. Yu, G. Chen, Q.-F. Wu, Y. Hsiao, C. L. Joe, J. X. Qiao, M. A. Poss, J.-Q. Yu, Ligand-enabled β-C(sp^3)–H olefination of free carboxylic acids. *J. Am. Chem. Soc.* **140**, 10363–10367 (2018).

(*64*) H. Chen, P. Wedi, T. Meyer, G. Tavakoli, M. van Gemmeren, Dual ligand-enabled nondirected C−H olefination of arenes. *Angew. Chem. Int. Ed.* **57**, 2497–2501 (2018).

(*65*) T. K. Achar, X. Zhang, R. Mondal, M. S. Shanavas, S. Maiti, S. Maity, N. Pal, R. S. Paton, D. Maiti, Palladium-catalyzed directed *meta*-selective C−H allylation of arenes: Unactivated internal olefins as allyl surrogates. *Angew. Chem. Int. Ed.* **58**, 10353–10360 (2019).

(*66*) K. K. Ghosh, A. Uttry, A. Mondal, F. Ghiringhelli, P. Wedi, M. van Gemmeren, Ligand-enabled γ-C(sp^3)−H olefination of free carboxylic acids. *Angew. Chem. Int. Ed.* (2020), doi:10.1002/anie.202002362.

(*67*) Z. Fan, K. L. Bay, X. Chen, Z. Zhuang, H. S. Park, K.-S. Yeung, K. N. Houk, J.-Q. Yu, Rational development of remote C−H functionalization of biphenyl: Experimental and computational studies. *Angew. Chem. Int. Ed.* **59**, 4770–4777 (2020).

(*68*) P. M. Osterberg, J. K. Niemeier, C. J. Welch, J. M. Hawkins, J. R. Martinelli, T. E. Johnson, T. W. Root, S. S. Stahl, Experimental limiting oxygen concentrations for nine organic solvents at temperatures and pressures relevant to aerobic oxidations in the pharmaceutical industry. *Org. Process Res. Dev*. **19**, 1537–1543 (2015).

(*69*) M. J. Frisch, G. W. Trucks, H. B. Schlegel, G. E. Scuseria, M. A. Robb, J. R. Cheeseman, G. Scalmani, V. Barone, B. Mennucci, G. A. Petersson, H. Nakatsuji, M. Caricato, X. Li, H. P. Hratchian, A. F. Izmaylov, J. Bloino, G. Zheng, J. L. Sonnenberg, M. Hada, M. Ehara, K. Toyota, R. Fukuda, J. Hasegawa, M. Ishida, T. Nakajima, Y. Honda, O. Kitao, H. Nakai, T. Vreven, J. A. Montgomery, Jr., J. E. Peralta, F. Ogliaro, M. Bearpark, J. J. Heyd, E. Brothers, K. N. Kudin, V. N. Staroverov, T. Keith, R. Kobayashi, J. Normand, K. Raghavachari, A. Rendell, J. C. Burant, S. S. Iyengar, J. Tomasi, M. Cossi, N. Rega, J. M. Millam, M. Klene, J. E. Knox, J. B. Cross, V. Bakken, C. Adamo, J. Jaramillo, R. Gomperts, R. E. Stratmann, O. Yazyev, A. J. Austin, R. Cammi, C. Pomelli, J. W. Ochterski, R. L. Martin, K. Morokuma, V. G. Zakrzewski, G. A. Voth, P. Salvador, J. J. Dannenberg, S. Dapprich, A. D. Daniels, O. Farkas, J. B. Foresman, J. V. Ortiz, J. Cioslowski, and D. J. Fox, Gaussian 09, Revision D.01, Gaussian, Inc., Wallingford CT, (2009).

(*70*) P. J. Hay, W. R. Wadt, Ab initio effective core potentials for molecular calculations. Potentials for the transition metal atoms Sc to Hg. *J. Chem. Phys.* **82**, 270-283 (1985).
(*71*) W. R. Wadt, P. J. Hay, Ab initio effective core potentials for molecular calculations. Potentials for main group elements Na to Bi. *J. Chem. Phys*. **82**, 284-298 (1985).
(*72*) A. D. Becke, Density-functional exchange-energy approximation with correct asymptotic behavior. *Phys. Rev. A*. **38**, 3098-3100 (1988).
(*73*) C. Lee, W. Yang, R. G. Parr, Development of the Colle-Salvetti correlation-energy formula into a functional of the electron density. *Phys. Rev. B*. **37**, 785-789 (1988).
(*74*) A. D. Becke, A new mixing of Hartree–Fock and local density-functional theories. *J. Chem. Phys.* **98**, 1372-1377 (1993).
(*75*) S. Grimme, J. Antony, S. Ehrlich, H. Krieg, A consistent and accurate ab initio parametrization of density functional dispersion correction (DFT-D) for the 94 elements H-Pu. *J. Chem. Phys.* **132**, 154104 (2010).
(*76*) E. Cancès, B. Mennucci, J. Tomasi, A new integral equation formalism for the polarizable continuum model: Theoretical background and applications to isotropic and anisotropic dielectrics. *J. Chem. Phys.* **107**, 3032-3041 (1997).
(*77*) B. Mennucci, J. Tomasi, Continuum solvation models: A new approach to the problem of solute's charge distribution and cavity boundaries. *J. Chem. Phys.* **106**, 5151-5158 (1997).
(*78*) G. Scalmani, M. J. Frisch, Continuous surface charge polarizable continuum models of solvation. I. General formalism. *J. Chem. Phys.* **132**, 114110 (2010).
(*79*) M. Dolg, U. Wedig, H. Stoll, H. Preuss, Energy-adjusted ab initio pseudopotentials for the first row transition elements. *J. Chem. Phys.* **86**, 866-872 (1987).
(*80*) M. Simonetti, D. M. Cannas, A. Panigrahi, S. Kujawa, M. Kryjewski, P. Xie, I. Larrosa, Ruthenium-Catalyzed C−H Arylation of Benzoic Acids and Indole Carboxylic Acids with Aryl Halides. *Chem. Eur. J.* **23**, 549–553 (2017).
(*81*) G. Cai, Y. Fu, Y. Li, X. Wan, Z. Shi, Indirect *ortho* Functionalization of Substituted Toluenes through *ortho* Olefination of N, N-Dimethylbenzylamines Tuned by the Acidity of Reaction Conditions. *J. Am. Chem. Soc*. **129**, 7666–7673 (2007).
(*82*) J.-C. Zhang, J.-L. Shi, B.-Q. Wang, P. Hu, K.-Q. Zhao, Z.-J. Shi, Direct Oxidative Arylation of Aryl C–H Bonds with Aryl Boronic Acids via Pd Catalysis Directed by the *N*,*N*-Dimethylaminomethyl Group. *Chem. Asian J.* **10**, 840–843 (2015).

Acknowledgments: We thank Jin-Quan Yu (Scripps), Donna Blackmond (Scripps), and other members in the NSF Center for C–H Functionalization for stimulating discussions during the course of this project. We also appreciate valuable discussions with Joshua Buss and David Bruns (UW-Madison). **Funding:** C.A.S. was supported by an NSF predoctoral fellowship (DGE-1747503), and other financial support was provided by NSF under the CCI Center for C–H Functionalization (CHE-1700982). Spectroscopic instrumentation was supported by a gift from Paul J. Bender, NSF (CHE-1048642), and NIH (1S10 OD020022-1), and the authors gratefully acknowledge the use of resources of the Cherry L. Emerson Center for Scientific Computation (Emory University).

Author contributions: S.S.S conceived the project in collaboration with C.A.S., who performed the experimental work and led primary data interpretation and analysis. K.N.F. and P.S.Z. assisted with collecting kinetic data and reaction optimization data. Computations were performed by B.E.H. and D.G.M. All work was done in consultation with D.G.M. and S.S.S. **Competing interests:** The authors declare no competing interests. **Data and materials availability:** All data are available in the main text or the supplementary materials.

Supplementary Materials:

Materials and Methods

Figures S1to S54

Table S1

References (*33-82*)